Available online at www.sciencedirect.com

SciVerse ScienceDirect

Ceramics International 38 (2012) 2957–2961

CERAMICS INTERNATIONAL

www.elsevier.com/locate/ceramint

Structure and thermal conductivity of yttria-stabilized hafnia ceramic coatings grown on nickel-based alloy

M. Noor-A-Alam, C.V. Ramana *

Department of Mechanical Engineering, University of Texas at El Paso, El Paso, TX 79968, United States

Received 3 October 2011; received in revised form 26 November 2011; accepted 26 November 2011
Available online 6 December 2011

Abstract

Yttria-stabilized hafnia (YSH) coatings were produced by sputter-deposition onto nickel (Ni) based super alloy substrates. The deposition was made by varying the growth temperature from room-temperature (RT) to 500 °C. The microstructure and thermal properties of the YSH coatings were evaluated employing grazing incidence X-ray diffraction (GIXRD), scanning electron microscopy (SEM), energy dispersive X-ray spectrometry (EDS) and phot-acoustic measurements. GIXRD studies indicate that the coatings grown at RT are amorphous while those grown at 300 °C and higher are crystalline. The crystalline YSH coatings crystallize in cubic hafnia phase and exhibit slightly enhanced lattice parameter compared to pure hafnia. The average grain size increases with increasing growth temperature. Thermal measurements indicate an effective reduction in thermal conductivity of YSH coatings compared to pure hafnia.

Keywords: C. Thermal conductivity; Yttria-stabilized hafnia; High-temperature ceramics; Thermal barrier coatings; Structure

1. Introduction

The ceramic materials, which can be employed as thermal barrier coatings (TBCs) and high-temperature oxidation resistance coatings, find wide spread applications in advanced technological applications such as gas turbines and aero engines [1–13]. The ceramic coatings primary function is to insulate and protect the metallic surface from high temperature exposure of the gas turbine or aero engine. These coatings are usually made of high-temperature tolerance ceramic materials, which can be applied as a thin layer over the metallic surface which makes insulation between the components and very high temperature environment. The ceramic coatings thus help the structural material to sustain at ambient temperature for prolonged time which consequently allows very high operating temperature. As the efficiency of the gas turbine depends on the operating temperature, the temperature tolerance of the TBC should be as high as possible to maximize the efficiency [1,2]. Additionally, different fuel compositions ranging from natural gas to broad range of syngas with high hydrogen contents are being tried for next generation gas turbine power plants. Therefore, the TBC candidate ceramic material for next generation gas turbine system should have the reliability and durability in diverse chemical, thermal and mechanical environment. Extensive efforts have been directed in last two decades towards the development of appropriate TBCs for gas turbine systems [1–13]. The commonly used materials for TBCs at present are based on yttria (Y_2O_3) stabilized zirconia (ZrO_2) namely YSZ, which has tolerance up to 1200 °C for long time operation. The phase transformation at temperature higher than 1200 °C which is associated with the volume change and development of cracks on the surface and interface of the TBC and substrate limits the application of YSZ at temperature more than 1200 °C [14]. The rigorous effort to increase the efficiency of gas turbine system led the scientific and engineering community to the exploration for better TBCs that will allow further increase the operating temperature. The hafnia (HfO_2) based TBCs have the potential to meet the requirement to be used in next generation gas turbine materials [15,16]. This postulation is mainly based on three important characteristics of hafnia namely similar crystal structure and phase transformation behavior to zirconia (ZrO_2), higher melting point (2900 °C), lower thermal conductivity and excellent radiation stability [17,18]. If realized, nanostructured hafnia

* Corresponding author. Tel.: +1 9157478690.
E-mail address: rvchintalapalle@utep.edu (C.V. Ramana).

0272-8842/$36.00
doi:10.1016/j.ceramint.2011.11.073

based TBCs are also associated with the reduction in weight of the TBCs which is a crucial factor in designing gas turbine rotating components. The impetus for this work is to fabricate and characterize the hafnia-based nanostructured coatings onto nickel (Ni) based super alloy substrates. Specifically, the attention is focused towards developing a fundamental understanding of the growth behavior, crystal structure, surface morphology and thermal conductivity of hafnia based coatings. The results obtained on the structure and thermal conductivity of YSH coatings are presented and discussed in this paper.

2. Experimental

Yttria-stabilized hafnia (YSH) coatings were produced using RF magnetron sputtering method. YSH coatings were grown onto Ni-based super alloy Inconel-738 (1.2 cm × 1.2 cm × 3 mm) substrates. The chamber was initially evacuated to a base pressure of ∼0.21 mPa. YSH target (5 cm diameter, 0.40 cm thick) (Plasmaterials Inc.) was used for sputtering. The composition of yttria in YSH was maintained at 7.5 mol% (7.5 YSH). The YSH target was placed on a 2-in. sputter gun, which was correspondingly placed at a distance of 8 cm from the substrate. A sputtering power of 30 W was initially applied to the target while introducing high purity argon (Ar) into the chamber causing plasma ignition. Once ignited, the power was increased to 100 W to deposit the coatings. The flow of the Ar was controlled using MKS mass flow meter. Before each deposition, the YSH-target was pre-sputtered for 10 min using Ar keeping the shutter above the gun closed. The samples were deposited at various temperatures (T_s) in the range of RT-500 °C. Coatings were grown to obtain a thickness of ∼1 μm. The substrates were heated by halogen lamps and the desired temperature was controlled by an Athena X25 controller. The fabrication conditions are summarized in Table 1.

Structural characterization of the coatings was performed by using X-ray diffraction (XRD) performed using a Bruker D8 Advance X-ray diffractometer. All the measurements were made ex-situ as a function of the coatings' fabrication conditions. XRD patterns were recorded using Cu Kα radiation (λ = 1.54056 Å) at RT. Surface imaging with scanning electron microscopy (SEM) was performed using a Hitachi S-4800 electron microscope. The thickness of the coatings was measured from the cross sectional imaging analysis performed by SEM. Thermal conductivity of the coatings was measured using photo-acoustic (PA) method, where a laser beam operating at a wavelength of 0.8 μm was used as the heating source. The laser is periodically irradiated on the sample surface. The substrate material and the additional surrounding medium layer are considered to be thermally thick compared to the YSH coating. The laser beam is concentrated using a mirror and directed to the YSH sample, which is mounted at the bottom of the PA cell. The condenser microphone senses the PA signal and transfers it to the lock-in amplifier, which is used to measure the amplitude and phase of the acoustic signal. A least square fitting procedure is used to determine unknown thermal conductivity and thermal contact resistance. The phase shift of the PA signal at each experimental frequency is calculated using the trial value of unknown properties.

Table 1
The YSH coating fabrication conditions.

Deposition parameter	Set value
Base pressure	∼0.21mPa
Sputtering pressure	∼0.50 Pa
Target	YSH (5 cm × 0.40 cm)
Substrate	Inconel-738
Substrate temperature	RT-500 °C
Target substrate distance	8 cm
RF power	100 W
Coating thickness	∼1 μm

3. Results and discussion

3.1. Crystal structure

XRD patterns of YSH coatings are shown in Fig. 1. The patterns indicate that the YSH coatings crystallize in cubic structure of hafnia. It is evident that the effect of growth temperature is not very significant on the phase except with an increase in the average grain size. The coatings exhibit oriented growth along (1 1 1) direction. It is evident from the XRD patterns (Fig. 1) that the (1 1 1) peak becomes sharper with increasing growth temperature. A decrease in the full-width at half-maximum (FWHM) associated with an intensity increase of the peak can be noted in the XRD data (Fig. 1). This observation clearly indicates that the crystallinity and the

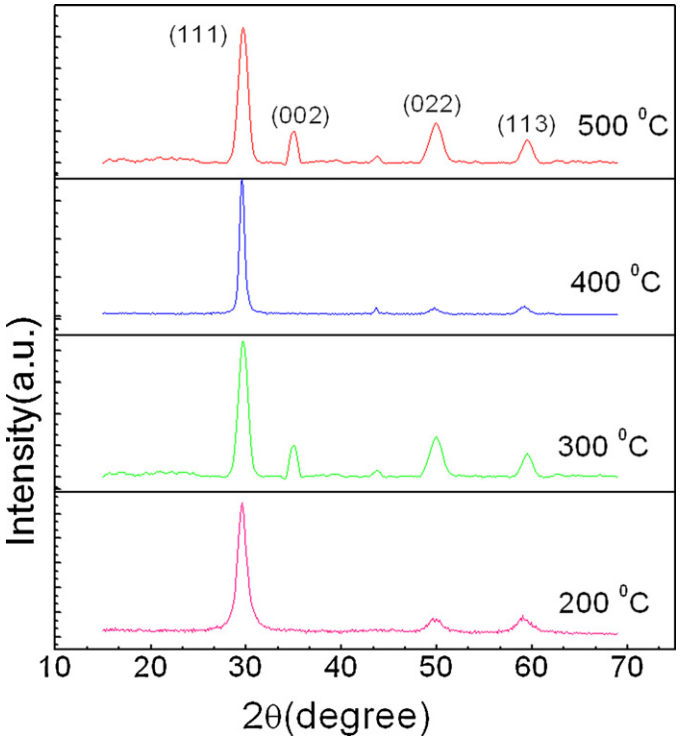

Fig. 1. XRD patterns of YSH coatings. It is evident from the XRD patterns that the coatings exhibit the cubic hafnia phase.

average grain size increases with increasing growth temperature. The lattice parameter determined for YSH coatings from XRD patterns is 0.52 nm, which is in agreement with that of cubic hafnia [19]. However, a slightly enhanced lattice parameter in YSH coatings compared to pure hafnia is due to the effect of Y^{3+} ions leading to lattice distortion. The ionic radii of Y^{+3}(0.1019 nm) is larger than that of Hf^{+4} (0.083 nm) which enforce the elongation of bond with oxygen in close proximity [20].

3.2. Surface morphology

The SEM images indicating the surface morphology of the YSH coatings are shown in Fig. 2. The morphology of the coatings is characterized by thin, elongated triangular network of grains connected together to form the dense surface structure. Based on the XRD and SEM data, it seems that a temperature of 300 °C is the critical temperature to promote ordered, oriented growth of YSH coatings. At this temperature the grains are fully grown and uniformly distributed across the sample surfaces. Triangular shaped grains, which are oriented in a specific morphology as seen in the SEM micrographs, provides the characteristic dense structure of the YSH coatings. For thick YSH coatings, Matsumoto et al. have reported that the morphology is characterized by the presence of triangular shaped grains on the surface [15,17]. In the present case, it seems that the signature of that characteristic is present although the coating thickness and size are significantly lower.

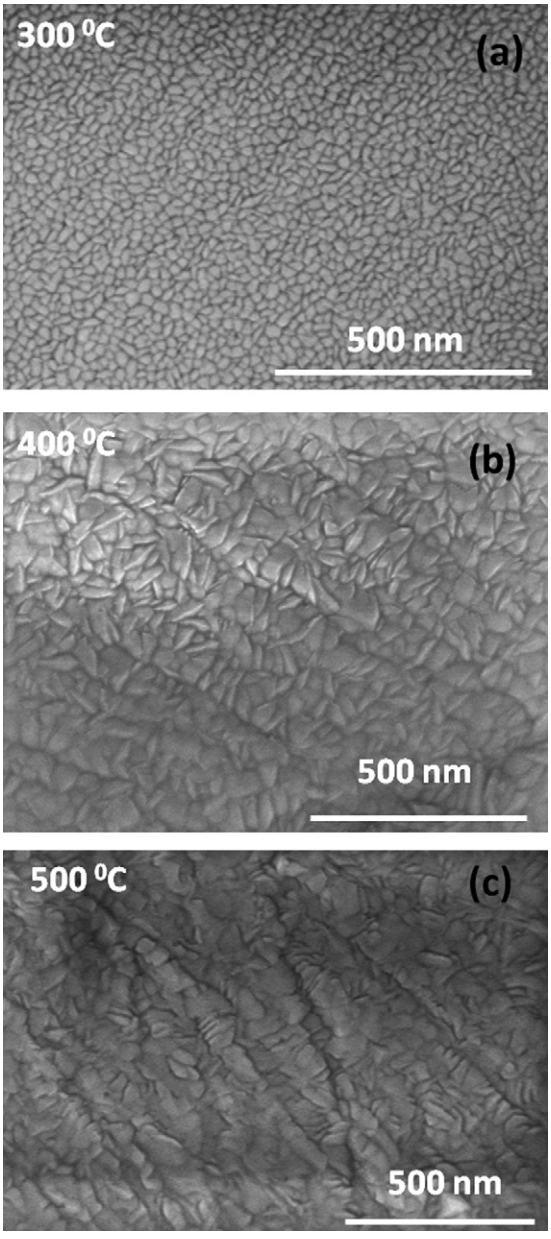

Fig. 2. SEM images of YSH coatings on Inconel-738 substrates. A slight increase in grain size and densification with increasing growth temperature can be noted.

The average grain size variation, determined from SEM imaging analysis, with growth temperature is shown in Fig. 3. It is evident that the grain size increases with increasing growth temperature which can be explained as follows. If temperature is low such that the period of the atomic jump process of adatoms on the substrate surface is very large, the condensed species may stay stuck to the regions where they are landing thus leading to an amorphous material formation in the coatings. The adatom mobility on the surface increases with increasing temperature, an important theromodynamic parameter in ceramic materials [21,22]. Thus the crystal structure and well defined grain size with increasing temperature can be attributed to the effect of temperature, which increases the mobility of the surface species to account for the observed results shown in Figs. 1–3.

3.3. Composition

It is important to verify that the composition of the coatings is retained similar to the target and compositional stability as a function of growth temperature. The EDS spectrum of the YSH coating is shown in Fig. 4. The EDS curve indicates the x-rays emitted from various elements. The peaks corresponding to Y, Hf, and O atoms present in the sample are as labeled (Fig. 4).

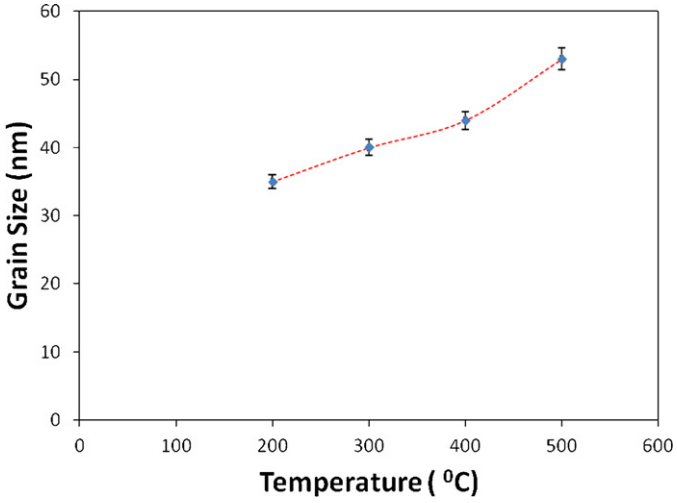

Fig. 3. Grain size variation with growth temperature in YSH coatings. Line is provided to guide the eye.

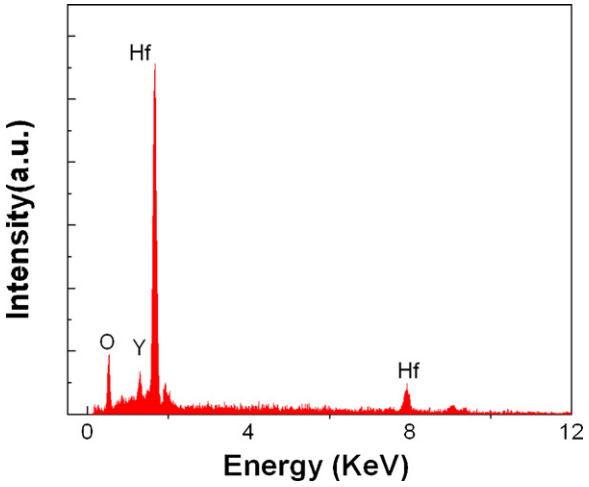

Fig. 4. EDS spectrum of YSH coatings grown at 500 °C. The X-ray peaks due to Y, Hf and O atoms and their respective positions are as indicated for the EDS curve. The data indicates a stoichiometric composition of the YSH coatings similar to the bulk of the target material.

The respective energy positions and the specific X-ray lines from various elements are also indicated in Fig. 4. The absence of any other peaks except from Y, Hf, and O indicate the YSH coatings without any elemental impurities incorporated during chemical processing and/or post-fabrication handling. The composition was very close to the starting composition of the target indicating the effective transfer of the stoichiometry during deposition of the coating.

3.4. Thermal conductivity

According to the thermal diffusion model (Rosencwaig–Gersho theory [23]), for an optically opaque sample, the expression for PA signal is:

$$\delta P = \frac{\gamma P_o I_o (\alpha_g \alpha_s)^{1/2}}{2\pi l_g T_o k_s f \sinh(l_s \sigma_s)} \exp\left[j\left(\omega t - \frac{\pi}{2}\right)\right] \quad (1)$$

where γ is the air specific heat ratio, P_o, the ambient pressure, T_o, the ambient temperature, I_o, the absorbed light intensity and $\omega = 2\pi f$, where f is the modulation frequency and l_i, k_i and α_s are the length, thermal conductivity and the thermal diffusivity of the sample, respectively. Here the subscript i (=s, g) denotes sample (s) and gas (g) medium. $\sigma_i = (1+j)a_i$ is the complex thermal diffusion coefficient of the material where $a_i = (\omega/2\alpha s)^{1/2}$. If the sample is thermally thick then Eq. (1) reduces to,

$$\delta P \cong \frac{\gamma P_o I_o (\alpha_g \alpha_s)^{1/2} (\exp - l_s (\pi f/\alpha_s)^{1/2}/f)}{\pi l_g T_o k_s} \times \exp\left[j\left(\omega t - \frac{\pi}{2} - l_s \alpha_s\right)\right] \quad (2)$$

where l_s is the thickness of the sample. From Eq. (2), amplitude varies as:

$$\left(\frac{1}{f}\right) \exp\left[l_s \left(\frac{\pi f}{\alpha_s}\right)^{1/2}\right] \quad (3)$$

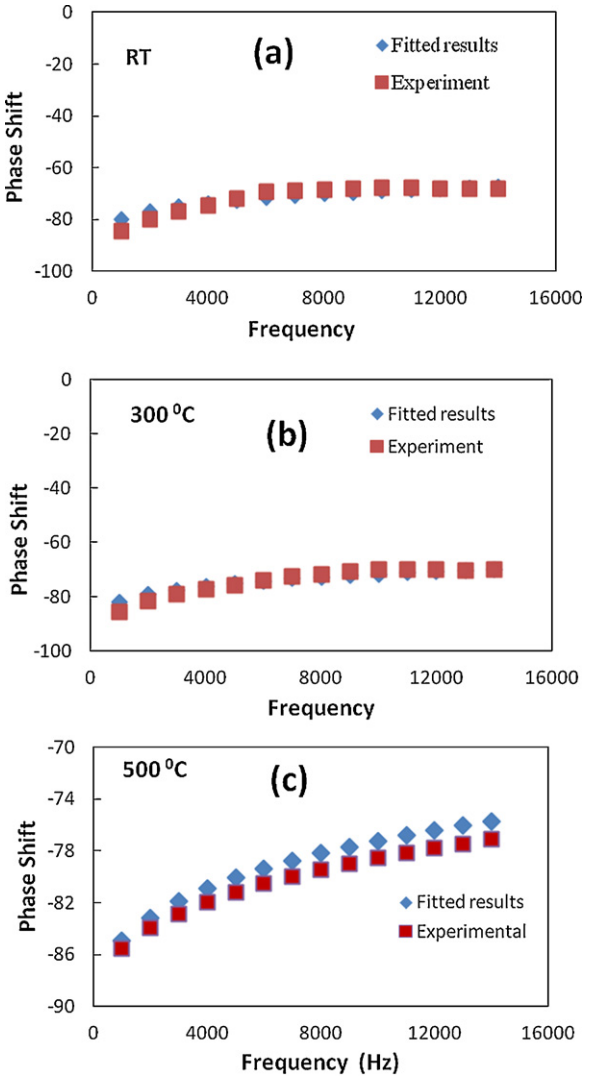

Fig. 5. Phase shift with respect to modulation frequency for YSH grown at RT (a), 300 °C (b) and 500 °C (c).

And phase varies as:

$$-l_s \left(\frac{\pi f}{\alpha_s}\right)^{1/2} \quad (4)$$

Hence, the thermal diffusivity can be measured either from amplitude data or from phase data.

The phase shift as a function of the modulation frequency for the YSH coatings is shown in Fig. 5. The thermal conductivity of YSH coatings are found within the range from 0.89 ± 0.03 to 1.3 ± 0.04 W/m-K. Fig. 6 shows the variation of thermal conductivity with respect to the temperature used for the growth of the YSH coatings. The two important observations that can be derived from thermal conductivity measurements of YSH coatings are as follows. The thermal conductivity of YSH coatings, in general, is lower than that of pure hafnia or bulk YSH is the first. The thermal conductivity slightly increases with increasing growth temperature is the later. The later behavior can be attributed to the increasing grain size with increasing growth temperature. Thermal diffusion through

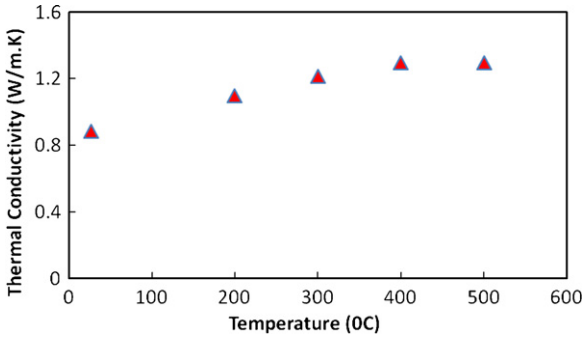

Fig. 6. Variation of thermal conductivity of YSH coatings with growth temperature.

lattice vibrations in a solid can be affected by: (a) phonon–phonon interactions, (b) imperfections, and (c) grain boundary scattering. The effective grain boundary decreases with increasing grain size leading to a decrease in phonon scattering and, hence, resulting in the observed increase in thermal conductivity. Effective reduction in the thermal conductivity of the YSH coatings grown at RT can be attributed to an amorphous structure, where there exist only smaller particles occasionally. The thermal conductivity increase with increasing grain size has been reported for YSZ [4,20]. On the other hand, the observed thermal conductivity decrease in yttria stabilized hafnia can be attributed to the addition of yttria to hafnia. Furthermore, thermal conductivity of YSH is much lower than that of pure hafnia. The reason for YSH materials exhibiting lower thermal conductivity than pure hafnia is the introduction of oxygen vacancies. These are structural vacancies in the hafnia crystals due to charge compensation of Y^{+3} ions substituting for Hf^{+4} ions. As a result, phonon scattering from the vacancies decreases effective thermal transport.

4. Conclusions

Yttria-stabilized hafnia (YSH) coatings were produced by sputter-deposition onto nickel (Ni) based super alloy substrates. The microstructure and thermal properties of the YSH coatings were evaluated. The coatings grown at RT are amorphous and exhibit lower thermal conductivity of 0.89 ± 0.03 W/m-K. The effective reduction in thermal conductivity in YSH coatings is noted. YSH coatings grown at 300 °C and higher are crystalline. The thermal conductivity increases to 1.3 ± 0.04 W/m-K with increasing grain size due to effective reduction in the grain boundary scattering.

Acknowledgements

This material is based upon work supported by the Department of Energy under Award Number DE-FE0000765.

References

[1] I. Gurrappa, A. Sambasiva, Thermal barrier coatings for enhanced efficiency of gas turbine engines, Surf. Coat. Technol. 201 (2006) 3016–3029.
[2] N.P. Padture, M. Gell, E.H. Jordan, Thermal barrier coatings for gas–turbine engine applications, Science 296 (2002) 280–284.
[3] A.G. Evans, D.R. Mumm, J.W. Hutchinson, G.H. Meier, F.S. Pettit, Mechanisms controlling the durability of thermal barrier coatings, Prog. Mater. Sci. 46 (2001) 505–553.
[4] G. Soyez, J.A. Eastman, L.J. Thomson, G.R. Bai, P.M. Baldo, A.W. McCormick, R.J. DiMelfi, A.A. Elmustafa, M.F. Tambwe, D.S. Stone, Grain-size-dependent thermal conductivity of nanocrystalline yttria stabilized zirconia films grown by metal-organic chemical vapor deposition, Appl. Phys. Lett. 77 (2000) 1155–1157.
[5] N. Wang, C. Zhou, S. Gong, H. Xu, Heat treatment of nanostructured thermal barrier coating, Ceram. Int. 33 (2007) 1075–1081.
[6] G.D. Girolamo, F. Marra, C. Blasi, E. Serra, T. Valente, Microstructure, mechanical properties and thermal shock resistance of plasma sprayed nanostructured zirconia coatings, Ceram. Int. 37 (2011) 2711–2717.
[7] D. Zhu, R.A. Miller, Sintering and creep behavior of plasma-sprayed zirconia- and hafnia-based thermal barrier coatings, Surf. Coat. Technol. 108 (1998) 114–120.
[8] L. Shaw, D. Goerman, R. Ren, M. Gell, The dependency of microstructure and properties of nanostructured coatings on plasma spray conditions, Surf. Coat. Technol. 130 (2000) 1–8.
[9] X. Cao, R. Vassen, W. Fischer, F. Tietz, W. Jungen, D. Stover, Lanthanum–cerium oxide as a thermal barrier coating for high temperature applications, Adv. Mater. 15 (2003) 1438–1442.
[10] R.S. Lima, A. Kucuk, C.C. Berndt, Evaluation of microhardness and elastic modulus of thermally sprayed nanostructured zirconia coatings, Surf. Coat. Technol. 135 (2001) 166–172.
[11] Z. Zhu, L. He, X. Chen, Y. Zhao, R. Mu, S. He, X. Cao, Thermal cycling behavior of $La_2Zr_2O_7$ coating with the addition of Y_2O_3 by EB-PVD, J. Alloys Compd. 508 (2010) 85–93.
[12] Z.-G. Liu, J.-H. Ouyang, B.H. Wang, J. Liu, Preparation and thermophysical properties of $Nd_xZr_{1-x}O_{2-x/2}$ ($x = 0.1$, 0. 2, 0. 3, 0. 4, 0. 5) ceramics, J. Alloys Compd. 466 (2008) 39–44.
[13] B. Saruthan, P. Francois, K. Fritcher, U. Schulz, EB-PVD processing of pyrochlore-structured $La_2Zr_2O_7$-based TBCs, Surf. Coat. Technol. 182 (2004) 175–183.
[14] W. Ma, D. Mack, J. Malzbender, R. Vaben, D. Stover, Yb_2O_3 and Gd_2O_3 doped strontium zirconate for thermal barrier coatings, J. Eur. Ceram. Soc. 28 (2008) 3071–3081.
[15] K. Matsumoto, Y. Itoh, T. Kameda, EB-PVD process and thermal properties of hafnia-based thermal barrier coating, Sci. Technol. Adv. Mater. 4 (2003) 153–158.
[16] H. Ibegazene, S. Alperine, C. Diot, Yttira-stabilized hafnia–zirconia thermal barrier coatings: the influence of hafnia addition on TBC structure and high temperature behavior, J. Mater. Sci. 30 (1995) 938–951.
[17] K. Matsumoto, Y. Itoh, Y. Ishiwata, Thermal conductivity and sintering behavior of hafnia-based thermal barrier coating using EB-PVD, in: International Gas Turbine Congress (IGTC) Proceedings (2003), Tokyo, Japan, November 2–7, (2003), p. 131.
[18] F. Kadlec, P. Simon, High-temperatrue infrared reflectivity of yttria-stabilized hafnia single crystals, Mater. Sci. Eng. B 72 (2000) 76.
[19] R. Terki, G. Bertrand, H. Aourag, C. Coddet, Cubic-to-tetragonal phase transition of HfO_2 from computational study, Mater. Lett. 62 (2008) 1484–1486.
[20] M.R. Winter, D.R. Clarke, Thermal conductivity of yttria-stabilized zirconia–hafnia solid solutions, Acta Mater. 54 (2006) 5051–5059.
[21] N.R. Kalidindi, F.S. Manciu, C.V. Ramana, Crystal structure, phase, and electrical conductivity of nanocrystalline $W_{0.95}Ti_{0.05}O_3$ thin films, ACS Appl. Mater. Int. 3 (2011) 863–868.
[22] V.H. Mudavakkat, M. Noor-A-Alam, K. Kamala Bharathi, S. AlFiafy, K. Dissanayeke, A. Kayani, C.V. Ramana, Structure and AC conductivity of nanocrystalline Yttrium oxide thin films, Thin Solid Films 519 (2011) 7947–7950.
[23] A. Rosencwaig, A. Gersho, Theory of the photoacoustic effect with solids, J. Appl. Phys. 47 (1976) 64–69.